

Aqueous Ring-Opening Polymerization-Induced Self-Assembly (ROPISA): Tailoring Anisotropic Nanoparticles through Amino Acid *N*-Carboxyanhydride (NCA) Monomer Selection

Hannah Beauseroy, Fatemeh Salimi, Julien Aujard-Catot, Léna Alembik, Sébastien Lecommandoux,* and Colin Bonduelle*



Cite This: *Macromolecules* 2025, 58, 6466–6479



Read Online

ACCESS |



Metrics & More

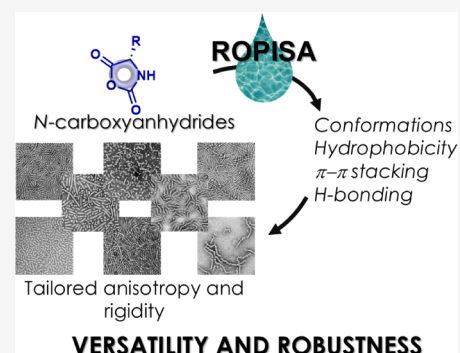


Article Recommendations



Supporting Information

ABSTRACT: The synthesis of anisotropic nanoparticles by polymerization-induced self-assembly (PISA) remains challenging yet holds significant potential for biomedical applications. In this context, aqueous ring-opening polymerization-induced self-assembly (ROPISA) of *N*-carboxyanhydrides (NCAs) has emerged as a promising strategy, offering a straightforward route to peptide-based nanomaterials. The present study was undertaken to evaluate the versatility of aqueous ROPISA across a range of NCAs, elucidating how their hydrophobicity and the chemical structure of the lateral chains provide access to nanoparticle anisotropy. A comparative analysis was conducted between NCAs with different protecting groups and those derived from distinct hydrophobic amino acids. Beyond hydrophobicity, the aqueous ROPISA of glycine NCA, phenylalanine NCA, and tyrosine NCA revealed the crucial role of additional factors such as the hydrophilic/hydrophobic balance, π - π stacking interactions, and hydrogen bonding in shaping nanoparticle anisotropy. Overall, this work highlights the broad applicability of aqueous ROPISA across a wide range of NCA monomers and its ability to generate tailored worm-like nanoparticles for advanced applications.



INTRODUCTION

Polymerization-induced self-assembly (PISA) has emerged as a highly versatile method in the field of dispersion polymerization, enabling the synthesis of well-defined nano-objects in a single-step process and at high concentrations.^{1,2} The PISA process results in the formation of amphiphilic block copolymers that self-assemble *in situ*, leading to the generation of self-stabilized nanoparticles with diverse morphologies (e.g., spheres, worms, vesicles), eliminating the need for additional surfactants.^{3–6} These morphologies can be controlled by modifying intrinsic parameters, including the chemical nature of the polymer segments,⁷ the solvophilic/solvophobic ratio,^{8,9} the architecture of the copolymer,^{10,11} and the molar mass dispersity. Additionally, other important factors, including the solvent,¹² pH, salt concentration,^{13,14} monomer concentration,¹⁵ temperature,¹⁶ stirring rate,¹⁴ and initiator concentration,¹⁷ can also influence the morphology of the nanoparticles.

PISA has been proposed as a highly attractive method for the development of drug delivery systems (DDS) used in nanomedicine,^{18–20} where size, dispersity, and shape control are critical factors. Especially, the use of anisotropic nanoparticles (i.e., nanoparticles with a length-to-width ratio greater than 1) shows great promise for further development of DDS. Indeed, several studies have demonstrated that anisotropic rod-like nanoparticles exhibit longer blood circulation half-life and

enhanced cellular internalization compared to their isotropic spherical counterparts.^{21–25} Despite this, the controlled formation of anisotropic nanoparticles using PISA remains limited to a narrow range of conditions that rely solely on hydrophilic-to-hydrophobic balance.²⁶ The PISA process has alternatively been extended to other supramolecular interactions, such as hydrogen bonding,²⁷ electrostatic interactions,²⁸ π - π interactions,²⁹ crystallization³⁰ and liquid crystal interactions.³¹ This has enabled the formation of anisotropic nanostructures with larger aspect ratios.

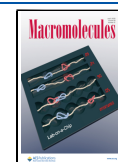
The study of PISA has been predominantly conducted within the frameworks of reversible addition–fragmentation chain transfer (RAFT) polymerization,³² atom-transfer radical polymerization (ATRP),³³ and nitroxide-mediated polymerization (NMP).³⁴ With these approaches, the scope of vinyl-based monomers that enable a PISA process in pure aqueous solutions remains restricted, and the majority of PISA processes require the use of organic solvents.^{35,36} Moreover,

Received: April 28, 2025

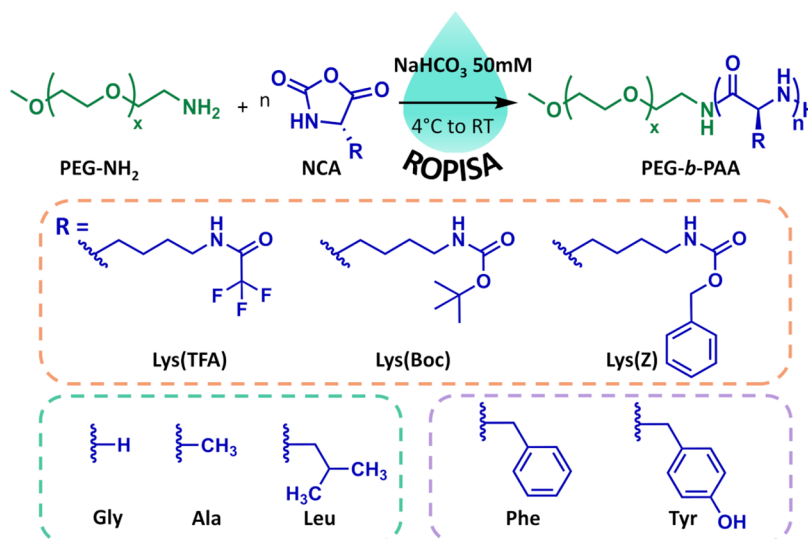
Revised: June 12, 2025

Accepted: June 16, 2025

Published: June 23, 2025



Scheme 1. Schematic Representation of Aqueous Ring-Opening Polymerization-Induced Self-Assembly (ROPISA) with a Range of Amino Acid *N*-Carboxyanhydrides used as Monomers (Orange: Influence of the Protecting Group; Green: Influence of the Hydrophobicity; and Purple: Influence of the π - π Stacking)



PISA-based radical polymerization processes mostly result in vinyl-based nanomaterials, constraining their applicability to further biomedical applications. For instance, the nondegradable nature of the nanomaterials raises concerns about toxic accumulation, as they cannot be metabolized or excreted, potentially leading to adverse effects. This highlights the need for better control over the fate of nanoparticles *in vivo*, prompting the design of fully (bio)degradable and biocompatible polymer assemblies. In this regard, the recent emergence of ring-opening PISA (ROPISA) of lactones,^{37,38} cyclic carbonates,³⁹ amino acid *N*-carboxyanhydrides (NCA),^{40–42} and *O*-carboxyanhydrides⁴³ offers promising new solutions.

We have recently reported a distinctive PISA process occurring in pure aqueous solutions that yields the formation of peptidic nanomaterials: the aqueous ROPISA of γ -benzylglutamate and leucine *N*-carboxyanhydrides (NCA).^{42,44} Despite the sensitivity of NCA to moisture, the issue of monomer hydrolysis and subsequent uncontrolled polymerization^{45,46} was addressed by adjusting the reaction conditions (pH and solids content) to allow for the ring opening by the amine propagating species to occur at a faster rate than hydrolysis, due to micellization and confinement of the polymerization. In addition, the aqueous phase enabled the synthesis of protein–polymer conjugates and nanomaterials composed entirely of amino acids, displaying protein-like properties.^{47–49} As with other PISA processes, the aqueous ROPISA of NCA is a method that enables anisotropic nanoparticles, the shape of which can be controlled by the chirality of the monomer and/or the secondary structure of the polypeptide block.⁵⁰ Nevertheless, only a limited number of monomers have been investigated so far,^{48,50,51} and the conventional principles of PISA, such as varying the hydrophilic/hydrophobic block ratio or concentration to achieve diverse morphologies, are elements that remain to be studied in this context.

Herein, we explore the versatility of this approach by investigating the aqueous ROPISA of various NCA monomer structures displaying different hydrophobicity, π - π stacking, H-bonding interactions, and the ability to stabilize polypeptide conformation when polymerized (Scheme 1). First, the

aqueous ROPISA of lysine monomers bearing different protecting groups (benzyloxycarbonyl, Z; trifluoroacetyl, TFA; and *tert*-butyloxycarbonyl, Boc) was studied and compared. We found that the choice of the protecting group for an amino acid could be a means of influencing the anisotropy by promoting good monomer dispersion, hydrophobicity, and π - π stacking during the propagation. Subsequently, to gain insight into the influence of side-chain hydrophobicity, glycine, alanine, leucine, and phenylalanine NCAs were subjected to further investigation. Interestingly, all these monomers produced anisotropic nanomaterials, and we clearly observed that varying hydrophobicity, as well as π - π stacking or H-bonding ability, impacted the kinetics of the ROP and the aspect ratio of the resulting nanomaterials. Finally, to specifically decipher the influence of π - π stacking, the polymerization of phenylalanine NCA and tyrosine NCA, both emerging amino acids for designing DDS,^{51,52} were subjected to a comprehensive study. With these two monomers, we confirmed that the tuning of anisotropy is driven not only by the hydrophobicity of the monomer alone but also by the π - π stacking interactions of the side chains and the overall hydrophilic/hydrophobic ratio. Altogether, our results highlight the versatility of aqueous ROPISA in designing wormlike nanoparticles, a morphology achievable with numerous NCA monomers (eight in this study). Moreover, side-chain functionalities serve as a key leverage to fine-tune the length-to-width ratio and rigidity.

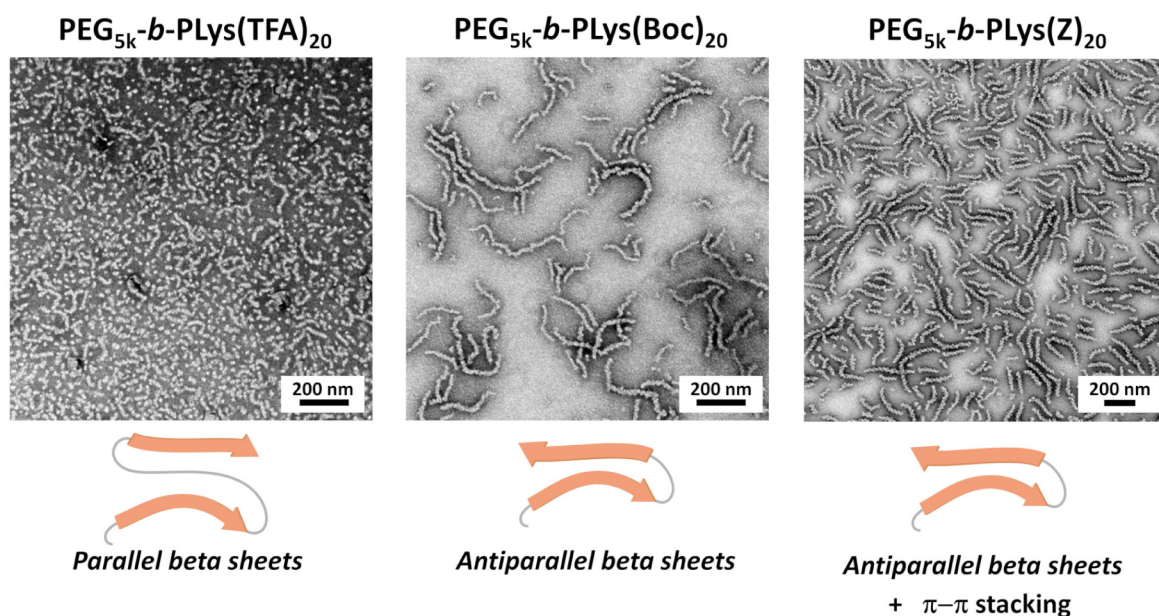
RESULTS AND DISCUSSION

ROPISA is Influenced by the Chemical Nature of the Protecting Groups. Although recent advances in ROP have enabled the rapid generation of polypeptides with predictable molar masses (M_n), low dispersity (\mathcal{D}), and well-defined reactive end groups, the synthesis of NCA monomers and their polymerization usually requires the use of organic solvents and, therefore, amino acid units with protected side chains.⁵³ We first investigated the influence of protecting groups with varying steric hindrance and water solubility on the aqueous ROPISA of three lysine-derived NCA monomers, all known to stabilize similar conformations: ϵ -trifluoroacetyl-*L*-lysine-NCA

Table 1. Macromolecular Characteristics of Diblock Copolymers Obtained by Aqueous ROPISA with Different Monomers, Using α -Amino Poly(ethylene Glycol) as a Macroinitiator, at a Feeding Ratio of 20

Copolymer	Monomer	Theory	SEC		¹ H NMR		Yield (%)	DLS	
		M_n [g mol ⁻¹]	M_n [g mol ⁻¹]	\bar{D}	M_n [g mol ⁻¹]	DP		D_z [nm] (σ) ^e	
PEG _{5k} - <i>b</i> -PLys(TFA) ₂₀	<i>L</i> -NTFALys	9200	13 100 ^a	1.06 ^a	10 400 ^c	24 ^c	77	114 ± 2 (0.21 ± 0.01)	
PEG _{5k} - <i>b</i> -PLys(Boc) ₂₀	<i>L</i> -NBocLys	9400	12 100 ^a	1.05 ^a	10 000 ^c	22 ^c	82	92 ± 3 (0.38 ± 0.04)	
PEG _{5k} - <i>b</i> -PLys(Z) ₂₀	<i>L</i> -NZLys	9900	13 900 ^a	1.12 ^a	10 800 ^c	22 ^c	92	101 ± 2 (0.15 ± 0.02)	
PEG _{5k} - <i>b</i> -PGly ₂₀	Gly	6100	49 100 ^b	1.07 ^b	6400 ^d	25 ^d	56	265 ± 8 (0.53 ± 0.02)	
PEG _{5k} - <i>b</i> -PAla ₂₀	<i>L</i> -Ala	6400	33 600 ^b	1.07 ^b	6500 ^d	21 ^d	73	149 ± 1 (0.41 ± 0.03)	
PEG _{5k} - <i>b</i> -PLeu ₂₀	<i>L</i> -Leu	7200	9200 ^a	1.03 ^a	7400 ^d	21 ^d	90	101 ± 2 (0.34 ± 0.05)	
PEG _{5k} - <i>b</i> -PPhe ₂₀	<i>L</i> -Phe	7900	9000 ^a	1.03 ^a	8200 ^d	22 ^d	79	85 ± 1 (0.27 ± 0.02)	
PEG _{5k} - <i>b</i> -PTyr ₂₀	<i>L</i> -Tyr	8200	9400 ^a	1.07 ^a	7600 ^c	16 ^c	89	77 ± 4 (0.23 ± 0.1)	

^aNumber-average molar-mass (M_n) and molar-mass dispersity determined by SEC in DMF + 1% LiBr using PS calibration. ^bIn HFIP + 0.05% KTFA using PMMA calibration. ^cNumber-average molar-mass (M_n) and degree of polymerization (DP) determined by ¹H NMR in DMSO-*d*₆. ^dIn TFA-*d*. ^eHydrodynamic diameter (D_z) and polydispersity (σ) determined by DLS at 90°.

**Figure 1.** Representative TEM images of the different copolymer nanoparticles obtained with Lys(TFA), Lys(Boc), and Lys(Z) at an initial $[M]/[I]$ ratio of 20, initiated by PEG_{5k}-NH₂, with corresponding parameters influencing the anisotropy.

(Lys(TFA)-NCA), ϵ -*tert*-butyloxycarbonyl-*L*-lysine-NCA (Lys(Boc)-NCA), and ϵ -benzyloxycarbonyl-*L*-lysine-NCA (Lys(Z)-NCA).⁵⁴ The aqueous ROPISA was conducted for each monomer using α -amino-poly(ethylene glycol) (PEG_{5k}-NH₂) as the macroinitiator in an ice-cold aqueous sodium bicarbonate solution (pH 8.5, 50 mM) with 20 equiv of NCA monomer, under vigorous stirring conditions. In all three cases, the NCA monomers were fully converted within a few hours, as evidenced by ¹H NMR spectroscopy and SEC chromatography. The resulting SEC chromatograms exhibited a monomodal distribution with narrow molar mass dispersity values, and the retention times shifted to lower values compared with the PEG macroinitiator, confirming effective block extension. Moreover, ¹H NMR spectra indicated that block copolymers exhibited similar degrees of polymerization (DP) values ranging from 22 to 24 (see Table 1, Figures 1 and S1–S3). Following dialysis against water to remove salts, the nanomaterial suspensions were characterized by using microscopy and light scattering techniques. Dynamic light scattering (DLS) analyses revealed the presence of nanoparticles with Z-average diameters of 101 nm for PEG_{5k}-*b*-

PLys(Z)₂₀, 92 nm for PEG_{5k}-*b*-PLys(Boc)₂₀ and 114 nm for PEG_{5k}-*b*-PLys(TFA)₂₀, with polydispersity index values of 0.15, 0.38, and 0.21, respectively (Table 1 and Figure S4). In the case of nanoparticles with anisotropic shapes, DLS yields sphere-equivalent hydrodynamic sizes, which might not be a good representation of the actual particle's dimensions. We attempted to determine translational and rotational diffusion coefficients without success using models appropriate for strongly anisotropic nanoparticles.⁵⁵ The anisotropic shape of our nanoparticles was instead revealed by imaging the opalescent solutions obtained by ROPISA using transmission electron microscopy (TEM). For the three NCA monomers, the microscopy images established the presence of worm-like nanoparticles (Figure 1) and approximately 50 nanoparticles were randomly selected and compared to statistically analyze the length and width of the nanomaterials (Figure S5).

Remarkably, anisotropic nanoparticles were obtained with all 3 monomers. TEM imaging with PEG_{5k}-*b*-PLys(TFA)₂₀ exhibited a coexistence of spherical micelles and necklace-type nanoparticles with a total mean length of 59 ± 37 nm and a width of 21 ± 4 nm, while in TEM imaging of PEG_{5k}-*b*-

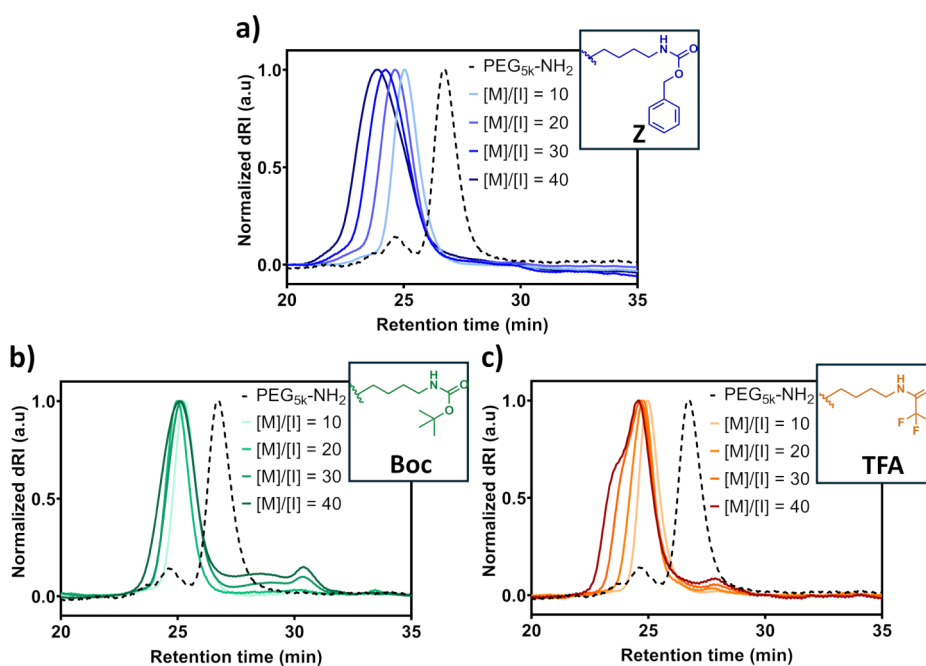


Figure 2. Size exclusion chromatograms of (a) $\text{PEG}_{5k}\text{-}b\text{-PLys}(\text{Z})_n$, (b) $\text{PEG}_{5k}\text{-}b\text{-PLys}(\text{Boc})_n$, and (c) $\text{PEG}_{5k}\text{-}b\text{-PLys}(\text{TFA})_n$ with targeted DP of 10, 20, 30, and 40 in DMF + 1% LiBr. (The peaks observed at lower mass, below the macroinitiator, were attributed to water-initiated ROP.)

$\text{PLys}(\text{Boc})_{20}$ suspensions, long and thick worm-like nanoparticles were observed, with a mean length of 116 ± 43 nm and a width of 30 ± 5 nm. As already reported by Liu et al.,⁵⁰ TEM imaging of $\text{PEG}_{5k}\text{-}b\text{-PLys}(\text{Z})_{20}$ displayed homogeneous superhelix-type nanoparticles of 173 ± 80 nm length and 38 ± 7 nm width. Overall, the DLS results and TEM imaging indicated that nanoparticles formed with the Z protecting group are longer and thicker than those with the *tert*-butyl carbamate (Boc) protecting group and more homogeneous than those with the trifluoroacetyl (TFA) group. As has been previously established, the influence of the secondary structure is an important factor that may guide the anisotropy upon ROPISA,⁴⁴ and to further elucidate this influence, we analyzed the lyophilized powder obtained with the 3 different monomer units using ATR-FTIR spectroscopy (see Figure S6).

With both Boc and Z protecting groups, the spectra demonstrated the presence of a prominent peak at 1630 cm^{-1} , which was attributed to the amide I and associated with a peak at 1530 cm^{-1} (the amide II region), along with a peak at 1690 cm^{-1} (side chain carbonyl). These stretchings corroborated the presence of an antiparallel β -sheet structure, a conformation that was previously associated with the formation of ribbon-like nanostructures.⁵⁰ In our ROPISA conditions, no notable differences in conformation were observed between the Boc and Z protecting groups. However, the anisotropic shapes of the nanomaterial exhibited significant variation (116 nm versus 173 nm), which we attributed to the π - π stacking introduced with Z. With TFA protecting groups, the ATR-FTIR spectra revealed that the amide I region exhibited a prominent peak at 1625 cm^{-1} , while the amide II region displayed peaks at 1555 cm^{-1} and 1540 cm^{-1} . These findings suggest that this last β -sheet structure was more constrained (i.e., parallel β -sheet),⁵⁶ which resulted in less pronounced anisotropy. Overall, the present study demonstrated that, besides the secondary structure, the dimension (parallel/antiparallel) and the chemical nature of the

protecting group (π - π stacking) could also be key parameters modulating the anisotropy.

To further investigate the influence of the overall hydrophilic/hydrophobic ratio with the 3 lysine derivatives, various aqueous ROPISA experiments were implemented using different feeding ratios (e.g., initial $[\text{M}]/[\text{I}]$ from 10 to 40) and α -amino-poly(ethylene glycol) ($\text{PEG}_{5k}\text{-NH}_2$) as the macroinitiator. The results of the ^1H NMR spectroscopy performed during ROPISA indicated that the $\text{PEG}_{5k}\text{-}b\text{-PLys}(\text{Z})$ block copolymers exhibited degrees of polymerization (DP) values ranging from 15 to 44, which were in close agreement with the targeted values (Table S1 and Figure S1). The corresponding SEC chromatograms exhibited a monomodal distribution with narrow molar mass dispersity values, and the retention times shifted to lower values compared to the PEG macroinitiator, confirming effective block extension (Figure 2a). DLS analysis revealed a progressive increase in the size of the nanoparticles (Figure S7) while TEM imaging showed the formation of heterogeneous helical ribbons for $\text{PEG}_{5k}\text{-}b\text{-PLys}(\text{Z})_{10}$. However, with an increasing Lys(Z) block length, larger aggregates were observed. Overall, anisotropic morphologies were obtained at specific hydrophilic/hydrophobic ratios, but increasing the length of the hydrophobic block resulted in uncontrolled aggregation. This highlights the critical balance needed in tuning block copolymer composition to achieve well-defined self-assembled structures with ROPISA of Lys(Z)-NCA.

In the absence of π - π stacking stabilization, the aqueous ROPISA of Lys(TFA)-NCA also led to the formation of copolymers whose degree of polymerization (DP), as determined by ^1H NMR, was found to be in agreement with the theoretical values (see Table S1 and Figure S2). However, beyond $\text{M}/\text{I} = 20$, SEC profiles (Figure 2b) exhibited peak splitting, which correlated with an increasing molar mass and the emergence of a peak at lower molar masses. This phenomenon suggested the formation of an oligomeric population generated through residual hydrolysis of NCA

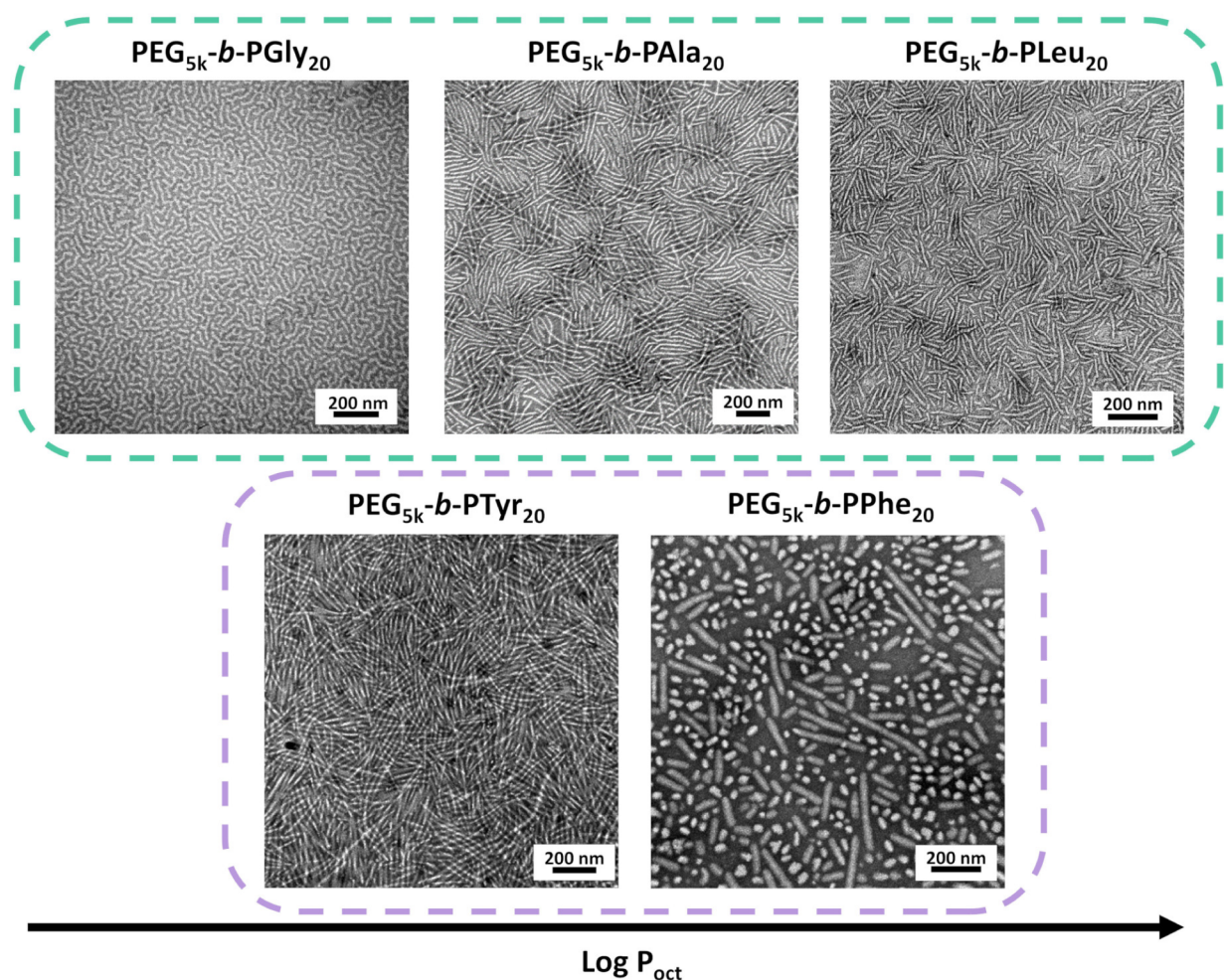


Figure 3. Representative TEM images of the different copolymer nanoparticles obtained with Gly, Ala, Leu, Phe, and Tyr at an initial $[M]/[I]$ ratio of 20, initiated by $\text{PEG}_{5k}\text{-NH}_2$. In green, the influence of the hydrophobicity, and in purple, the influence of the π - π stacking, with increasing $\text{Log } P_{\text{oct}}$.

monomers (“water-initiated”). This was attributed to less efficient dispersion of the NCA monomer in the aqueous phase, which could originate from the strong hydrophobic nature of TFA. Finally, the aqueous ROPISA of Lys(Boc)-NCA, displaying more steric hindrance than the two other lysine derivatives, led to the formation of copolymers whose degree of polymerization (DP), calculated by ^1H NMR, indicated that the molar masses remained unchanged at increasing feeding ratios (see Figure 2c, Table S1, and Figure S3). Moreover, the SEC profiles exhibited an increased number of oligomers formed through water initiation, suggesting that the polypeptide chains were unable to maintain an optimal propagation rate during ROPISA. Overall, comparing the aqueous ROPISA of Lys(TFA)-NCA, Lys(Boc)-NCA, and Lys(Z)-NCA demonstrated that the hydrophobicity of the different protecting groups significantly influenced the polymerization process and the anisotropy. At higher $[M]/[I]$, water initiation was observed with Lys(TFA)-NCA and Lys(Boc)-NCA. Moreover, we found that the benzyl group facilitated superior dispersion of the monomer powder in an aqueous medium and favored a more pronounced anisotropic shape through π - π stacking. All of these factors, in turn, enabled a more regulated aqueous polymerization and self-assembly for Lys(Z)-NCA, which resulted in a more

uniform distribution of nanoparticles than that observed with Boc- and TFA-protected groups.

ROPISA is Influenced by the Hydrophobicity of the Amino Acid Side Chain. The study of lysine derivatives with different protecting groups clearly showed that the hydrophobicity of the side chain can play an important role in the ROPISA process and modulate the anisotropy of the nanoparticles obtained. To better evaluate this influence, we selected a series of 5 NCA monomers: glycine NCA, alanine NCA, tyrosine NCA, leucine NCA, and phenylalanine NCA, arranged in order of increasing hydrophobicity, with calculated $\text{Log } P_{\text{oct}}$ values of -0.31 , 0.02 , 1 , 1.33 , and 1.48 , respectively.^{57–59} Alanine NCA (Ala-NCA) was synthesized by the Leuchs method (Figure S8), while the others were commercially available. The aqueous polymerization was carried out under the same conditions as those previously used with lysine derivatives, with an initial feed ratio $[M]/[I]$ of 20. According to ^1H NMR spectroscopy, the different ROPISA processes afforded copolymers with DP values similar to the targeted ones (Table 1 and Figures S9–S13). SEC analyses demonstrated that well-defined amphiphilic block copolymers with a narrow dispersity ($\mathcal{D} < 1.2$) were consistently produced, confirming the effectiveness of aqueous ROPISA at low $[M]/[I]$ for all hydrophobic monomers and,

surprisingly, even for the nonhydrophobic monomer glycine NCA (Table 1 and Figures S14–S18).

Following purification, the suspensions of nanoparticles were analyzed by DLS and imaged by TEM. For PEG_{5k}-*b*-PGly₂₀, DLS showed sizes with high dispersity ($\sigma \approx 0.5$) (Figure S19), likely due to the nanoparticles' morphology. Indeed, TEM images revealed the presence of wormlike nanoparticles resembling flexible fibrils, both simple and branched, with an average diameter of 13 ± 2 nm (Figures 3 and S20). The lengths of these fibrils could not be determined because of the variability in branching. Atomic force microscopy (AFM) was also conducted and confirmed this fibril morphology (Figure S21).

It is important to note that the glycine monomer was fully soluble at the initial stage of the ROPISA process and that the aggregation of the polypeptide is attributable to its ability to form intermolecular hydrogen bonds and other dipolar interactions, such as CO–CO interactions.⁶⁰ Interestingly, the sphere-equivalent Z-average diameter of the nanoparticle suspensions was found to be larger for PEG_{5k}-*b*-PALA₂₀ than for PEG_{5k}-*b*-PLeu₂₀, although the dispersity was high ($\sigma > 0.2$) in both cases (Table 1, Figures 3, S22 and S23). For both NCA monomers, TEM revealed the presence of long, thin, and rod-like nanoparticles with homogeneous diameters (151 ± 58 nm in length and 11 ± 2 nm in diameter for PEG_{5k}-*b*-PALA₂₀; 102 ± 42 nm in length and 11 ± 2 nm in diameter for PEG_{5k}-*b*-PLeu₂₀, Figures 3, S24 and S25). PEG_{5k}-*b*-PALA₂₀ nanoparticles had a higher aspect ratio than PEG_{5k}-*b*-PLeu₂₀ nanoparticles. Nanoparticle suspensions prepared from PEG_{5k}-*b*-PPhe₂₀ exhibited a sphere-equivalent z-average diameter distribution that was more homogeneous, with a mean diameter of 85 ± 1 nm and a polydispersity index (σ) of 0.27 ± 0.02 (Table 1 and Figure S26). However, in marked contrast to the findings reported by Morrell et al. using a polysarcosine macroinitiator,⁴⁸ we observed by TEM a heterogeneous mixture of long and thick nanorods mixed with spherical micelles. The distribution of nanoparticles was rather heterogeneous in length (105 ± 82 nm), but the dispersion of diameters was narrow (26 ± 4 nm) (Figure S27).

Finally, DLS analyses of PEG_{5k}-*b*-PTyr₂₀ indicated a Z-average hydrodynamic diameter of 77 ± 4 nm (Figure S28). In comparison to PEG_{5k}-*b*-PPhe₂₀ having a more hydrophobic polypeptide block, this ROPISA yielded nanoparticles with a smaller diameter and a significantly lower proportion of spherical micelles, as shown by TEM (Table 1, Figures 3, and S29).

Beyond hydrophobicity, the influence of the secondary structure is an important factor that may also guide the anisotropy of the proposed 5 monomers. To further elucidate this influence, we also analyzed the lyophilized powder obtained upon ROPISA by using ATR-FTIR spectroscopy. First, glycine, the simplest and achiral amino acid, lacks the classic structural features of typical polypeptides affording secondary structure. However, glycine's specific conformational structure involving hydrogen bonding has already been reported and found to be similar to beta sheets.^{61,62} The spectrum displayed a prominent peak in the amide I region at 1644 cm^{-1} and another in the amide II region at 1560 cm^{-1} , which are characteristic of the poly(glycine II) (PGII) conformation—an extended helical structure commonly found in solution (Figure S30).^{61,63} In comparison, the FTIR spectrum of PEG_{5k}-*b*-PALA₂₀ showed a peak at 1625 cm^{-1} in the amide I region and at 1538 cm^{-1} in the amide II region,

indicating a β -sheet conformation. For PEG_{5k}-*b*-PLeu₂₀, a prominent peak at 1627 cm^{-1} and a smaller one at 1653 cm^{-1} in the amide I region, along with a peak at 1544 cm^{-1} in the amide II region, suggest a mix of β -sheet and α -helical structures (Figure S31). For all 3 monomers, the " β -sheet" conformation was likely responsible for the increased anisotropy observed, particularly when comparing alanine and leucine. FTIR analyses were also conducted on dried powders of PEG_{5k}-*b*-PPhe₂₀ and PEG_{5k}-*b*-PTyr₂₀ (Figure S32). The phenylalanine-based copolymer displayed a peak at 1632 cm^{-1} in the amide I region and at 1545 cm^{-1} in the amide II region, indicative of β -sheet structures. Similarly, the tyrosine-based copolymer exhibited characteristic peaks in both the amide I and II regions, also confirming the presence of β -sheet conformations. The observed anisotropic structures likely arise from the combined effects of hydrophobic interactions and the intrinsic β -sheet secondary structure of the polypeptides. As during a crystallization process,^{44,64} the β -sheet conformation provides a rigid and directional framework, while the degree of hydrophobicity also modulates the overall prominence of the anisotropy.

Recent studies carried out in organic solvents and with lactide suggest that the ROPISA process may be strongly influenced by ROP kinetics and that the speed of these kinetics, compared with self-assembly kinetics involving a CDSA process, may explain the formation of more anisotropic morphologies.⁶⁵ To better understand such an influence, aqueous ROPISA kinetics were studied by monitoring the different monomer conversions using ¹H NMR at a feed ratio of 20, initiated by PEG_{5k}-NH₂. HCl was used to quench polymerization at different time points (Figures S33–S37). Remarkably, in the case of glycine and alanine, the aqueous ROP was "superfast" and achieved in less than 5 min. Plots of $\ln([M]_0/[M]_t)$ versus time indicated a first-order dependence on the monomer concentration (Figure 4). A detailed investigation of polymerization kinetics yielded apparent kinetic rate constant (*k*) values of 1.52 min^{-1} and 1.535 min^{-1} , respectively. The *k* values obtained with leucine,

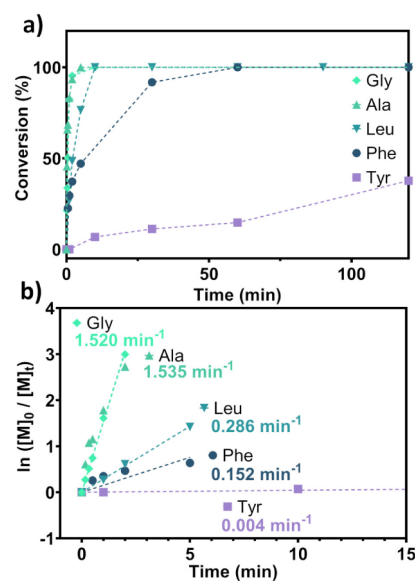


Figure 4. Kinetic profiles of (a) conversion vs time and (b) $\ln([M]_0/[M]_t)$ vs time at an initial $[M]_0/[I]$ ratio of 20 determined by ¹H NMR spectra.

Table 2. Macromolecular Characteristics of Diblock Copolymers Obtained by Aqueous ROPISA with Phe-Nca

Copolymer	Theory	SEC		¹ H NMR			Yield (%)	DLS
	M_n [g mol ⁻¹]	M_n [g mol ⁻¹] ^a	D^a	M_n [g mol ⁻¹] ^c	DP ^c	f_{PEG}^d		D_z [nm] (σ) ^e
PEG _{2k} - <i>b</i> -PPhe ₂	2300	3900	1.07	3200	8	0.62	9	-
PEG _{2k} - <i>b</i> -PPhe ₅	2800	3900	1.05	3600	11	0.55	50	113 ± 1 (0.27 ± 0.01)
PEG _{2k} - <i>b</i> -PPhe ₁₀	3500	4100	1.05	4200	15	0.48	86	102 ± 1 (0.26 ± 0.02)
PEG _{2k} - <i>b</i> -PPhe ₂₀	4900	ns ^b	ns ^b	5100	21	0.39	81	715 ± 55 (0.21 ± 0.16)
PEG _{5k} - <i>b</i> -PPhe ₂	5300	7000	1.07	5300	2	0.94	58	135 ± 5 (0.27 ± 0.01)
PEG _{5k} - <i>b</i> -PPhe ₅	5700	7400	1.07	5800	5	0.87	65	82 ± 2 (0.25 ± 0.01)
PEG _{5k} - <i>b</i> -PPhe ₁₀	6400	7900	1.07	6500	10	0.77	74	87 ± 1 (0.2 ± 0.01)
PEG _{5k} - <i>b</i> -PPhe ₂₀	7900	9000	1.03	8200	22	0.61	79	85 ± 1 (0.27 ± 0.02)
PEG _{10k} - <i>b</i> -PPhe ₂	10 300	18 400	1.02	10 400	3	0.96	82	253 ± 4 (0.48 ± 0.06)
PEG _{10k} - <i>b</i> -PPhe ₅	10 800	19 900	1.03	11 000	7	0.91	95	66 ± 2 (0.38 ± 0.04)
PEG _{10k} - <i>b</i> -PPhe ₁₀	11 500	19 900	1.03	11 500	10	0.87	76	80 ± 1 (0.37 ± 0.02)
PEG _{10k} - <i>b</i> -PPhe ₂₀	12 900	ns ^b	ns ^b	13 700	25	0.73	84	118 ± 1 (0.23 ± 0.04)

^aNumber average molar-mass (M_n) and molar-mass dispersity determined by SEC in DMF + 1% LiBr using PS calibration. ^bNot soluble in common SEC solvents. ^cNumber average molar-mass (M_n) and degree of polymerization (DP) determined by ¹H NMR in TFA-*d*. ^dHydrophilic fraction or PEG fraction determined by this equation $\frac{M_n^{\text{PEG}}}{M_n^{\text{copolymer}}}$ with M_n from ¹H NMR. ^eHydrodynamic diameter (D_z) and polydispersity (σ) determined by DLS at 90°.

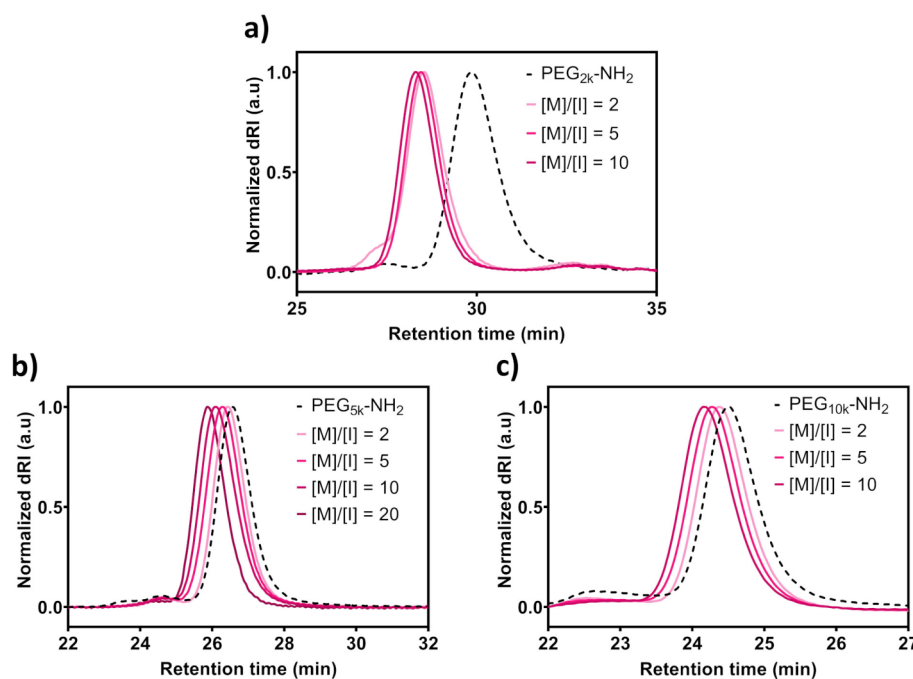


Figure 5. SEC profiles of (a) PEG_{2k}-*b*-PPhe_n, (b) PEG_{5k}-*b*-PPhe_n, and (c) PEG_{10k}-*b*-PPhe_n with targeted DP of 2, 5, 10, and 20 in DMF + 1% LiBr.

phenylalanine, and tyrosine NCAs were found to be slightly higher, with values of 0.286 min⁻¹, 0.152 min⁻¹, and 0.004 min⁻¹, respectively. This kinetic study indicates that the aqueous ROP kinetics are directly influenced by the hydrophobicity of the NCA monomer. Hypothetically, the more hydrophobic the monomer, such as phenylalanine NCA, the slower the dispersion and diffusion in the solid state. In addition, consistent with previous studies on the ROPI-CDSA of lactide, slower ROP kinetics observed with phenylalanine NCA and tyrosine NCA lead to reduced anisotropy. This could explain the coexistence of spherical and rod-like nanoparticles for these monomers.

In summary, aqueous ROPISA enables the polymerization of diverse NCA monomers with varying hydrophobicity. The hydrophobicity, chemical structure, and steric hindrance of

these monomers significantly influence polymerization kinetics and self-assembly behavior, and they provide organized spatial patterns induced by the specific polypeptide conformations.⁶⁶ In contrast to classical dispersion methods, such as RAFT-PISA in water, which may impose limitations on the available monomers, ROPISA appears to exhibit a wider range of monomer options. In RAFT-PISA, the hydrophobicity of core-forming monomers and their corresponding oligomers requires careful control.³⁵ In contrast, aqueous ROPISA accommodates a wider range of hydrophobic monomers as long as they are sufficiently dispersed to diffuse into the polymerization locus.

Besides Hydrophobicity, π - π Interactions versus Hydrophilic Content: Phenylalanine NCA. Our previous studies^{42,47} and the current investigation indicate that the majority of our ROPISA attempts result in the formation of

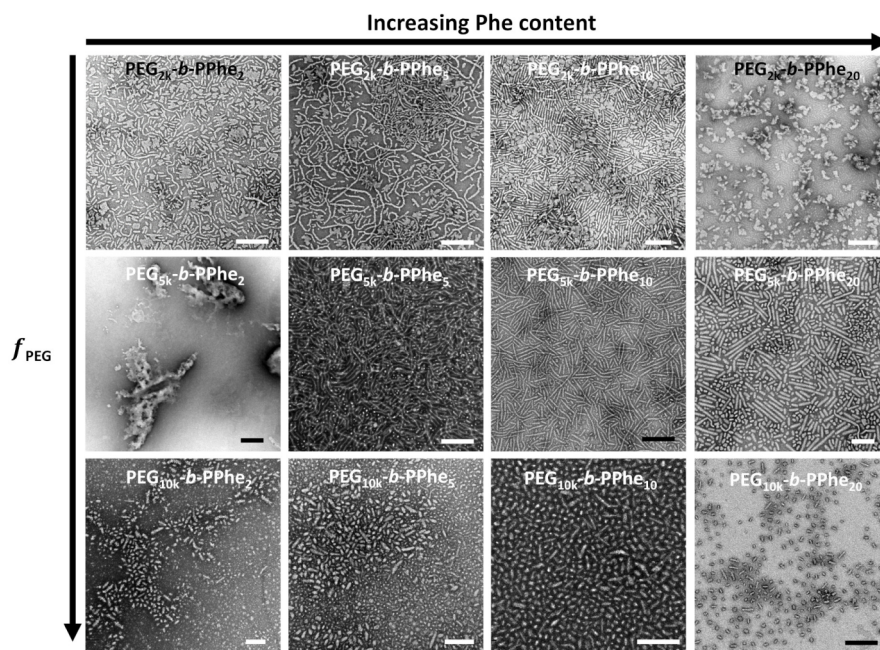


Figure 6. Representative TEM images of the different copolymer nanoparticles obtained with Phe, with different hydrophilic/hydrophobic block ratios and Phe contents (scale bar: 200 nm).

anisotropic nanomaterials, in marked contrast to other PISA processes. This specific behavior may be due to the significance of the packing provided by the polypeptide chains as a determining factor in the formation of this morphology.^{44,64,66} Nevertheless, nanoparticle solutions comprising $\text{PEG}_{5k}\text{-}b\text{-PPhe}_{20}$ and $\text{PEG}_{5k}\text{-}b\text{-PTyr}_{20}$ also exhibited the simultaneous formation of spherical micelles during ROP. This difference can be attributed to slower ROP kinetics, which are not amenable to a CDSA process, as shown by recent studies on lactide.⁶⁵ Indeed, the presence of spherical shapes suggests that self-assembly is closer to an equilibrium in which the amphiphilic character may have more influence. To determine whether the morphology could be influenced by the hydrophilic/hydrophobic ratio, we further investigated the ROPISA of Phe-NCA by varying the M/I ratio. The objective was also to decipher how the aromatic ring of the side chain of phenylalanine could arrange stabilizing $\pi\text{-}\pi$ interactions that are especially relevant in drug delivery applications.^{67,68} So far, the traditional ring-opening polymerization performed in organic solvent still presents significant challenges when used to polymerize Phe-NCA, and this monomer has been mainly studied in copolymerization systems.^{69–71} In a nonaqueous ROPISA approach, Du et al. investigated the fate of Phe-NCA in THF, initiated by $\text{PEG}_{2k}\text{-NH}_2$, and achieved the formation of polymersomes with a block ratio of 1:20 and a solid content of 20%.⁴⁰ Subsequently, Morrel et al. employed aqueous ROP to extend polysarcosine with Phe-NCA, with the objective of synthesizing a polymer with DP values ranging from 8 to 33. In this second case, the process also resulted in nanomaterials exhibiting anisotropic characteristics.⁴⁸

We first performed the aqueous ROPISA of Phe-NCA, utilizing a 2 kDa PEG amine macroinitiator, with the aim of targeting lower hydrophilic fractions than those already studied (Figure 3). The monomer powder was combined with the initiator using extensive stirring at 4 °C in a sodium bicarbonate aqueous buffer (pH 8.5, 50 mM) at monomer-to-initiator ratios of 2 (f_{PEG} of 0.6, $\text{PEG}_{2k}\text{-}b\text{-PPhe}_2$), 5 (f_{PEG} of

0.5, $\text{PEG}_{2k}\text{-}b\text{-PPhe}_5$), 10 (f_{PEG} of 0.4, $\text{PEG}_{2k}\text{-}b\text{-PPhe}_{10}$), and 20 (f_{PEG} of 0.3, $\text{PEG}_{2k}\text{-}b\text{-PPhe}_{20}$) and at a solid content of 7 wt %. Upon ROPISA, the solutions were dialyzed against ultrapure water (RC cutoff 1 kDa) for 2 days, with regular changes of water. NMR analyses confirmed the expected chemical structures and enabled the estimation of number-averaged molar mass M_n values that were slightly higher than the targeted values (Table 2 and Figure S38). Furthermore, the chain extension proceeded effectively, as demonstrated by the SEC chromatograms and corroborated by the low molar mass dispersity (\mathcal{D}) values between 1.05 and 1.07 (Figure 5a). Nanoparticle formation was confirmed by DLS and TEM analyses, even at a DP of 8, with a mixture of short rod and aggregate structures (Figures 6 and S39). As the length of the polypeptide block increased, the nanoparticles developed into progressively longer and more elongated structures at a DP of 11. At a DP of 15, the nanoparticles exhibited enhanced anisotropy, and at a DP of 20, they formed aggregates (Figure 6). To enhance the hydrophilic/hydrophobic ratio and examine its influence on the resulting nanoparticle morphology, we proceeded to conduct the aqueous ROPISA of Phe-NCA with the incorporation of 5 or 10 kDa PEG amine (f_{PEG} between 0.6 and 0.9, Table 2). The macroinitiator was combined with the monomer powder through extensive stirring at 4 °C in a sodium bicarbonate aqueous buffer (pH 8.5, 50 mM) at monomer-to-initiator ratios ranging from 2 to 20. In all instances, the NCA monomers underwent complete conversion, as substantiated by ^1H NMR spectroscopy. Additionally, ^1H NMR spectroscopy and SEC chromatograms demonstrated effective control over the polymerization process. The calculated DP values by ^1H NMR exhibited a high degree of correlation with the targeted values, as evidenced by the data presented in Table 2 (Figures S11, S40 and S41).

SEC analysis confirmed the effective extension of the PEG chains and the attainment of a low molar mass dispersity (ranging from 1.03 to 1.07) (Figure 5b,c). To further

Table 3. Macromolecular Characteristics of Diblock Copolymers Obtained by Aqueous ROPISA with Tyr-Nca

Copolymer	Theory			SEC		¹ H NMR			DLS	
	M_n [g mol ⁻¹]	M_n [g mol ⁻¹] ^a	D^a	M_n [g mol ⁻¹] ^b	DP ^b	f_{PEG}^c	Yield (%)	D_z [nm] (σ) ^d		
PEG _{5k} - <i>b</i> -PTyr ₁₀	6600	9300	1.05	6300	8	0.79	67	73 ± 3 (0.21 ± 0.01)		
PEG _{5k} - <i>b</i> -PTyr ₂₀	8200	9900	1.07	7500	15	0.67	85	77 ± 4 (0.23 ± 0.1)		
PEG _{5k} - <i>b</i> -PTyr ₃₀	10 100	11 100	1.15	9900	30	0.50	91	Gel		
PEG _{5k} - <i>b</i> -PTyr ₅₀	13 300	12 000	1.13	12 300	45	0.40	81	Gel		
PEG ₇₅₀ - <i>b</i> -PTyr ₂₀	3900	3300	1.46	4300	22	0.14	85	Aggregates		
PEG _{2k} - <i>b</i> -PTyr ₂₀	5200	5500	1.13	5300	20	0.46	84	560 ± 16 (0.21 ± 0.05)		
PEG _{10k} - <i>b</i> -PTyr ₂₀	13 300	22 200	1.06	17 700	47	0.56	46	441 ± 56 (0.75 ± 0.06)		

^aNumber average molar-mass (M_n) and molar-mass dispersity determined by SEC in DMF + 1% LiBr using PS calibration. ^bNumber average molar-mass (M_n) and degree of polymerization (DP) determined by ¹H NMR in in DMSO-*d*₆. ^cHydrophilic fraction or PEG fraction determined by this equation $\frac{M_n^{\text{PEG}}}{M_{n,\text{copolymer}}}$ with M_n from ¹H NMR. ^dHydrodynamic diameter (D_z) and polydispersity (σ) determined by DLS at 90°.

distinguish the influence of the polypeptide molar mass from any influence of the secondary structure, we also analyzed the lyophilized powder obtained via ROPISA using ATR-FTIR spectroscopy. The IR spectra of all copolymers, regardless of the size of the PEG component, exhibited β -sheet conformation, as evidenced by the presence of amide I and II peaks at 1630 cm⁻¹ and 1545 cm⁻¹ (see Figures S32, S42–S44).

Overall, good control over the polymerization was achieved when initiated with PEG5k and PEG10k, demonstrating effective chain extension, no water initiation, and a high yield. In contrast, initiation with PEG2k showed less control, resulting in lower yields and higher average DPs than targeted. This suggests the potential hydrolysis of Phe-NCA into its corresponding amino acid, which was subsequently removed by dialysis. Notably, no evidence of water initiation was observed in this case.

DLS analysis confirmed the presence of nanoparticles with a Z-average diameter ranging between 82 and 715 nm, with a relatively narrow size dispersity in the case of PEG_{5k} (Table 2, Figures S45 and S46). Overall, TEM observations of the different suspensions indicated that the PEG fraction exerted a significant influence on the morphology of the nanoparticles. Representative TEM imaging is depicted in Figure 6 as a function of PEG content or the π - π stacking ability.

First, the addition of a longer polypeptide block and the subsequent reduction of the hydrophilic fraction from 0.94 to 0.61 resulted in the formation of thicker anisotropic nanoparticles when PEG_{5k} was used (second line, Figure 6). The PEG_{5k}-*b*-PPhe₅ nanoparticles were characterized by a long, thin, and wormlike morphology. The PEG_{5k}-*b*-PPhe₁₀ nanoparticles were thicker and appeared more rigid; yet, they were also mixed with shorter nanoparticles. With a lower PEG fraction value of 0.61, PEG_{5k}-*b*-PPhe₂₀ exhibited thick anisotropic structures but was also mixed with spherical micelles. In comparison, when PEG_{10k} was used to increase the PEG fraction, the nanoparticles were shorter and exhibited a markedly reduced degree of anisotropy. This phenomenon was attributable to the increased curvature that results from the larger hydrophilic PEG block and the higher hydrophilic fraction (0.73–0.96). Indeed, an increase in the hydrophilic block size enhances the surface area in contact with the aqueous environment, thereby facilitating the formation of more spherical or less elongated structures. In marked contrast, when the hydrophilic ratio was lower, as observed in the case of PEG_{2k}-*b*-PPhe₂₀ ($f_{\text{PEG}} = 0.48$), the resulting nanoparticles exhibited reduced anisotropy and aggregate morphology. Additionally, despite having a similar hydrophilic fraction

close to 0.75, PEG_{10k}-*b*-PPhe₂₀ and PEG_{5k}-*b*-PPhe₁₀ displayed a distinct aspect ratio, with more anisotropy arising from lower PEG molar mass. The ROPISA of phenylalanine, using poly(ethylene glycol) initiators of different molar masses, demonstrated that controlled polymerization could be achieved, leading to the formation of nanoparticles with different aspect ratios. In this context, the tuning of anisotropy is not solely dependent on the secondary structure (as β -sheets are formed in all cases) or the monomer's hydrophobicity. It is also influenced by the hydrophilic/hydrophobic ratio and the π - π stacking interactions of phenylalanine. These findings highlight the potential of ROPISA as a powerful tool for generating anisotropic nanoparticles whose morphologies are tailored by various noncovalent interactions, including the use of monomers such as Phe-NCA, which are usually challenging to polymerize.

Toward More Functional π - π Interactions: Tyrosine NCA. In the field of nanomedicine, another NCA monomer of interest is derived from tyrosine, which shares similarities with phenylalanine. In contrast to phenylalanine, tyrosine features a polar side chain containing a phenol group. In drug delivery, this unique characteristic facilitates strong π - π stacking and H-bonding interactions with drug molecules.^{72,73} Aiming to design anisotropic nanomaterials made of this amino acid—a goal not yet achieved in the literature—an in-depth study was conducted on the aqueous ROPISA of tyrosine NCA and compared to phenylalanine. A series of block copolymers were synthesized by implementing the aqueous ROPISA using PEG_{5k}-NH₂ as the macroinitiator in an ice-cold aqueous sodium bicarbonate solution (pH 8.5, 50 mM) with 10, 20, 30, and 50 equiv of Tyr-NCA monomer, while stirring vigorously. These stoichiometries were chosen to best cover the different PEG fractions from 10% to 80% (see Table 3). It was noteworthy that for targeted DPs of 30 and 50, the aqueous medium exhibited gradual gelation over time. The gelation ability of tyrosine in aqueous media has been previously investigated for its potential applications in biomedical fields, including drug delivery.^{74–77} This encompasses the research conducted by Huang et al., who synthesized amphiphilic block copolymers based on PEG-*b*-(oligo)Tyr.⁷⁸ Previous research indicated that gelation properties were a result of the interaction between the polar phenolic side chains from the hydrophobic Tyr block.

Following purification, either from the gel or from the aqueous solution, the copolymers presented in Table 3 were subjected to analysis by ¹H NMR and SEC. The results of the ¹H NMR spectroscopy revealed that the average number molar mass (M_n) values were in agreement with the initial $[M]/[I]$

Increasing Tyr content, H-bonding

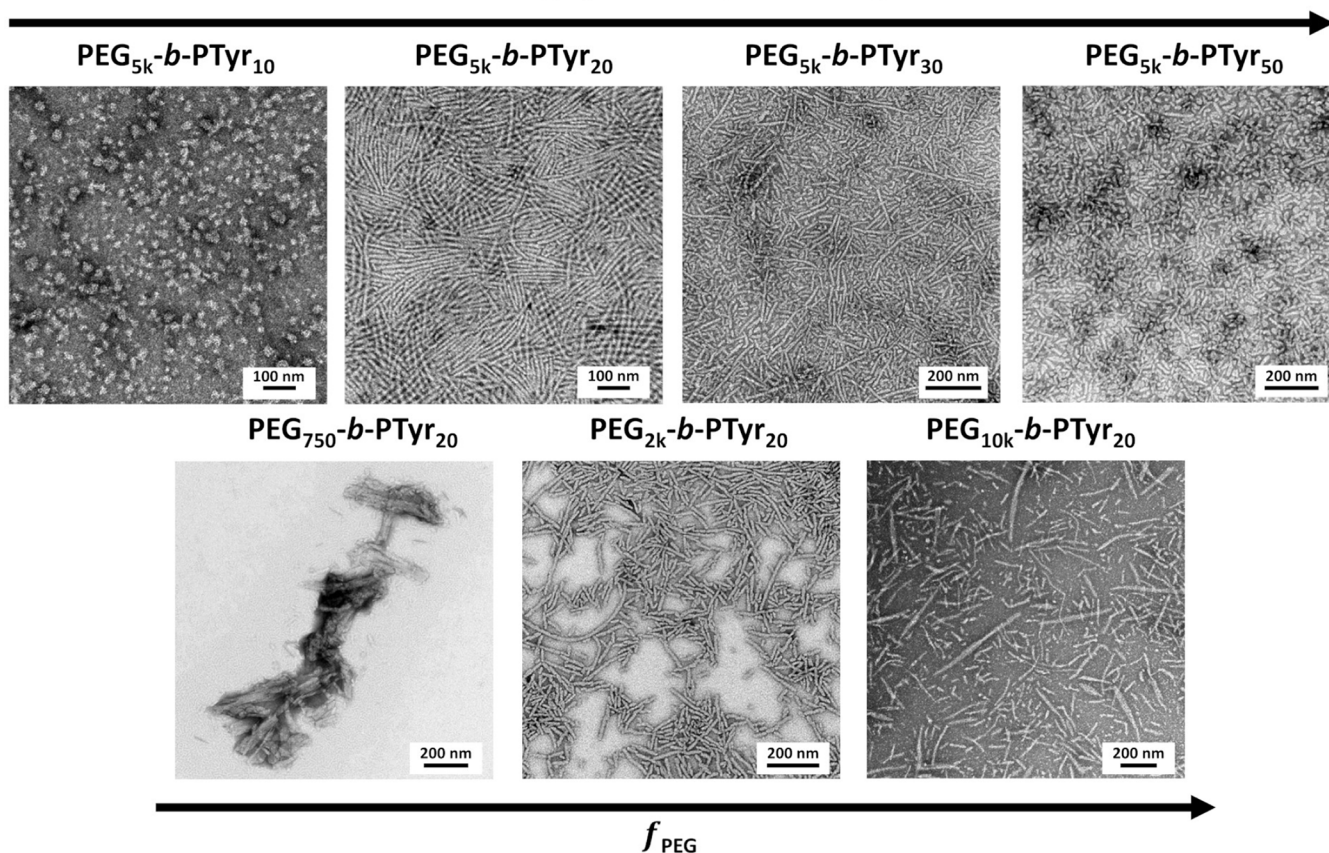


Figure 7. Representative TEM images of the different copolymer nanoparticles obtained with Tyr, with different hydrophilic/hydrophobic block ratios and Tyr contents and H-bonding.

ratio (Table 3, Figures S13 and S47). However, the SEC chromatograms indicated that as the $[M]/[I]$ ratio increased, there was a corresponding rise in the proportion of the population observed at higher retention times (Figure S48). We attributed these residual oligomer populations to water-initiated polytyrosine that may have been produced by the gelation of the medium during ROPISA, which likely reduced the efficiency of monomer dispersion when stirring ceased. We also conducted ATR-FTIR spectroscopy on the lyophilized powder obtained after ROPISA. All copolymers exhibited β -sheet conformation, an expected result, as evidenced by the presence of amide I and II peaks in their IR spectra (Figures S32 and S49).

Dynamic light scattering analysis of $\text{PEG}_{5k}\text{-}b\text{-PTyr}_{10}$ and $\text{PEG}_{5k}\text{-}b\text{-PTyr}_{20}$ revealed a narrow size distribution around 70 nm with a dispersity index of approximately 0.2 (Figure S50). However, TEM showed that $\text{PEG}_{5k}\text{-}b\text{-PTyr}_{10}$ formed spherical aggregates with an average diameter of 38 ± 8 nm (Figure S51) and $\text{PEG}_{5k}\text{-}b\text{-PTyr}_{20}$ produced long and thin nanoparticles mixed with spherical micelles, with an average length of 119 ± 83 nm and an average diameter of 12 ± 2 nm (Figure S29) as illustrated in Figure 3.

$\text{PEG}_{5k}\text{-}b\text{-PTyr}_{30}$ and $\text{PEG}_{5k}\text{-}b\text{-PTyr}_{50}$ could not be analyzed by DLS due to gel formation. However, TEM analysis revealed the presence of heterogeneous anisotropic nanoparticles, whose entanglement, along with hydrogen bonding,^{74–77} likely contributed to the gelation. These nanoparticles exhibited dimensions of 113 ± 71 nm in length for the targeted DP of 30

and 61 ± 33 nm for the targeted DP of 50, with widths of 11 ± 2 nm and 17 ± 7 nm, respectively (Figures 7 and S51–S53).

Achieving anisotropy control and modulation with tyrosine proves to be challenging.⁷⁸ Adjusting the feeding ratio during polymerization introduces additional complexities, including gel formation, which promotes water initiation and reduces control over polymerization. These factors result in less homogeneous self-assembled structures, highlighting the need for further optimization.

To better assess the influence of the PEG fraction, aqueous ROPISA was also attempted using PEG-NH₂ of different sizes, specifically 750 Da, 2 kDa, and 10 kDa, to vary the hydrophilic fraction as well as the number of tyrosine units (hydrophilic/hydrophobic ratio). ROPISA experiments were performed using ice-cold aqueous sodium bicarbonate buffer with a feeding ratio of 20. Following purification, ¹H NMR analysis was conducted, revealing that the DP values were close to the targeted ones, with the exception of PEG_{10k} which exhibited a higher molar mass than the theoretical value (see Table 3, Figures S54 and S55). In the SEC chromatograms, a shift to lower retention times confirmed the successful chain extension from the macroinitiator (Figure S56). $\text{PEG}_{750}\text{-}b\text{-PTyr}_{20}$ displayed a rather high molar mass dispersity ($\mathcal{D} = 1.46$) compared to the other copolymers, but this result was attributed to the high dispersity of the commercial $\text{PEG}_{750}\text{-NH}_2$ used in this experiment ($\mathcal{D} = 1.38$). For $\text{PEG}_{10k}\text{-}b\text{-PTyr}_{20}$, the presence of tyrosine oligomers was observed, likely due to the water-initiated polymerization of Tyr-NCA. At higher DP, NMR analyses indicated a loss of control over the

polymerization, confirming the SEC analyses. FTIR spectra revealed the presence of α -sheet amide I and II bands for all the copolymers (Figure S57).

The nanomaterial suspensions were characterized by using microscopy and light scattering techniques to assess the formation of anisotropic nanomaterials. PEG₇₅₀-*b*-PTyr₂₀, which has the lowest PEG fraction (f_{PEG} value of 0.14), displayed aggregates with a lamellar morphology in TEM (Figure 7). This morphology has already been reported by Jiang et al. with PEG_{2k}-*b*-PTyr₁₀ and upon nanoprecipitation.⁷⁹ Increasing the hydrophilic fraction while keeping the same targeted number of Tyr units appeared to stabilize the formation of elongated heterogeneous nanoparticles, as observed by TEM and DLS. PEG_{2k}-*b*-PTyr₂₀ nanoparticles (101 ± 51 nm, 15 ± 2 nm) were slightly thicker than PEG_{5k}-*b*-PTyr₂₀ (12 ± 2 nm) (Figures 7, S29, S58 and S59). For PEG_{10k}-*b*-PTyr₂₀, the nanoparticles were long but exhibited significant heterogeneity in length with a nanosheet morphology (see Figures 7 and S60). The significant anisotropy observed in the PEG_{10k}-*b*-PTyr₂₀ nanoparticles could be due to strong π - π interactions among the tyrosine residues, but the variation in their lengths suggests that the assembly process was not entirely uniform, possibly due to the lack of control during the ROPISA process.

Overall, the aqueous ROPISA of tyrosine NCA demonstrated that the PEG fraction, π - π stacking, and hydrogen bonding all influenced both the polymerization process and the resulting anisotropy. Indeed, aqueous ROPISA performed with tyrosine NCA afforded anisotropic nanomaterials with a complex influence of various factors beyond the secondary structure, hydrophobicity, π - π stacking, and hydrophilic/hydrophobic ratio. At higher M/I, water initiation and gel formation were observed, but we found conditions in which a more pronounced anisotropic shape could be induced. Eventually, additional factors, such as the amount of water-initiated polymerization, could have played a pivotal role in the process. However, in light of our SEC analyses, water-initiated polymerization seems modest at this stage under the proposed conditions, and the influence of this parameter was not studied in this work.

Summary of the Knowledge Gained from the Study.

The present study was undertaken to evaluate the versatility of aqueous ROPISA across a range of NCAs, elucidating how their hydrophobicity and the chemical structure of the lateral chains provide access to polypeptide-based nanoparticles. In the initial phase of the study, lysine NCAs with Z, Boc, and TFA protecting groups were investigated. A more regulated aqueous polymerization and self-assembly were found for Lys(Z)-NCA, which resulted in a more uniform distribution of nanoparticles than that observed with Boc- and TFA-protected groups. Subsequently, to gain insight into the influence of side chain hydrophobicity, glycine, alanine, leucine, and phenylalanine NCAs were subjected to further investigation. First, and unexpectedly, incorporating glycine—a hydrophilic monomer that polymerizes into aggregated polypeptides through hydrogen bonding alone—also resulted in the formation of worm-like nanoparticles, a behavior that was attributed to its specific nonchiral conformation. Nanoparticles derived from alanine exhibited greater anisotropy, which was attributed to a decrease in steric hindrance and a lower degree of hydrophobicity. The complexity of the system was then increased by introducing phenylalanine, a more hydrophobic amino acid that promotes π - π stacking, which is of great

interest in drug delivery. A comprehensive analysis was conducted by varying the size of both the hydrophilic poly(ethylene glycol) block and the hydrophobic polypeptide block, demonstrating that the hydrophilic/hydrophobic ratio and the number of phenylalanine units, which affect the extent of π - π stacking, had a significant impact on nanoparticle anisotropy. Similarly, the ability of tyrosine to influence nanoparticle morphology was examined, following the same approach used for phenylalanine. Tyrosine, with its phenol side chain, participates in π - π stacking and introduces hydrogen bonding, which is influenced by the pH of the medium. This property is advantageous in drug delivery applications, as it potentially improves drug loading content due to these dual interactions. These interactions, in conjunction with the hydrophilic–hydrophobic equilibrium, were demonstrated to influence both the polymerization and self-assembly processes. Overall, all the NCA monomers produced anisotropic nanomaterials, and we clearly observed that varying hydrophobicity, as well as π - π stacking or H-bonding ability, impacted the kinetics of the ROP and the aspect ratio of the resulting nanomaterials.

CONCLUSIONS

In summary, this study demonstrates the versatility and robustness of aqueous ROPISA, a process that can be applied with almost all NCA monomers identified so far and that affords a wide range of tailored anisotropic nanoparticles. The present study also elucidates how their hydrophobicity and the chemical structure of the lateral chains provide access to anisotropic nanoparticles. In fact, similar to lactide ROPICDSA in organic solvent,³⁸ aqueous ROPISA seems to offer privileged access to worm-like structures. Most notably, it highlights that factors such as hydrophobicity and steric hindrance, by influencing the polymerization kinetics, as well as π - π stacking, hydrophilic/hydrophobic ratio, and hydrogen bonding, serve as pivotal driving forces in regulating anisotropic self-assembly, in conjunction with secondary structure and monomer chirality.

ASSOCIATED CONTENT

Supporting Information

The Supporting Information is available free of charge at <https://pubs.acs.org/doi/10.1021/acs.macromol.5c01089>.

Additional experimental details, including materials and methods, synthetic protocols, kinetic studies; additional data, including ¹H NMR spectra, SEC chromatograms, ATR-FTIR spectra, DLS profiles, TEM images, and histograms (PDF)

AUTHOR INFORMATION

Corresponding Authors

Sébastien Lecommandoux – University Bordeaux, CNRS, Bordeaux INP, LCPO, UMR 5629, Pessac F-33600, France; Email: lecommandoux@enscbp.fr

Colin Bonduelle – University Bordeaux, CNRS, Bordeaux INP, LCPO, UMR 5629, Pessac F-33600, France;

orcid.org/0000-0002-7213-7861;

Email: colin.bonduelle@enscbp.fr

Authors

Hannah Beuseroy – University Bordeaux, CNRS, Bordeaux INP, LCPO, UMR 5629, Pessac F-33600, France

Fatemeh Salimi – University Bordeaux, CNRS, Bordeaux INP, LCPO, UMR 5629, Pessac F-33600, France
Julien Aujard-Catot – University Bordeaux, CNRS, Bordeaux INP, LCPO, UMR 5629, Pessac F-33600, France
Léna Alembik – University Bordeaux, CNRS, Bordeaux INP, LCPO, UMR 5629, Pessac F-33600, France

Complete contact information is available at:
<https://pubs.acs.org/10.1021/acs.macromol.5c01089>

Author Contributions

The manuscript was written with contributions from all authors. All authors have approved the final version of the manuscript.

Notes

The authors declare no competing financial interest.

ACKNOWLEDGMENTS

The authors acknowledge Amélie Vax and Sylvain Bourasseau for assistance with size-exclusion chromatography, and Paul Marque for assistance with ATR-FTIR and DLS. This work was supported by a grant overseen by the French National Research Agency (ANR, Grant No. ANR-20-CE06-0020-01). It was also conducted within the framework of the University of Bordeaux's IdEx "Investments for the Future" program RRI "Frontier of Life," which received financial support from the French government. Additionally, this work was supported by the Horizon Europe research and innovation program under grant agreement No. 101079482 ("SUPRALIFE").

REFERENCES

- (1) Penfold, N. J. W.; Yeow, J.; Boyer, C.; Armes, S. P. Emerging Trends in Polymerization-Induced Self-Assembly. *ACS Macro Lett.* **2019**, *8* (8), 1029–1054.
- (2) Zhao, Z.; Lei, S.; Zeng, M.; Huo, M. Recent Progress in Polymerization-Induced Self-Assembly: From the Perspective of Driving Forces. *Aggregate* **2024**, *5* (1), No. e418.
- (3) Takahashi, R.; Miwa, S.; Sobotta, F. H.; Lee, J. H.; Fujii, S.; Ohta, N.; Brendel, J. C.; Sakurai, K. Unraveling the Kinetics of the Structural Development during Polymerization-Induced Self-Assembly: Decoupling the Polymerization and the Micelle Structure. *Polym. Chem.* **2020**, *11* (8), 1514–1524.
- (4) Czajka, A.; Armes, S. P. In Situ SAXS Studies of a Prototypical RAFT Aqueous Dispersion Polymerization Formulation: Monitoring the Evolution in Copolymer Morphology during Polymerization-Induced Self-Assembly. *Chem. Sci.* **2020**, *11* (42), 11443–11454.
- (5) Derry, M. J.; Fielding, L. A.; Armes, S. P. Polymerization-Induced Self-Assembly of Block Copolymer Nanoparticles via RAFT Non-Aqueous Dispersion Polymerization. *Prog. Polym. Sci.* **2016**, *52*, 1–18.
- (6) Warren, N. J.; Mykhaylyk, O. O.; Mahmood, D.; Ryan, A. J.; Armes, S. P. RAFT Aqueous Dispersion Polymerization Yields Poly(Ethylene Glycol)-Based Diblock Copolymer Nano-Objects with Predictable Single Phase Morphologies. *J. Am. Chem. Soc.* **2014**, *136* (3), 1023–1033.
- (7) Ratcliffe, L. P. D.; Blanazs, A.; Williams, C. N.; Brown, S. L.; Armes, S. P. RAFT Polymerization of Hydroxy-Functional Methacrylic Monomers under Heterogeneous Conditions: Effect of Varying the Core-Forming Block. *Polym. Chem.* **2014**, *5* (11), 3643–3655.
- (8) Blanazs, A.; Ryan, A. J.; Armes, S. P. Predictive Phase Diagrams for RAFT Aqueous Dispersion Polymerization: Effect of Block Copolymer Composition, Molecular Weight, and Copolymer Concentration. *Macromolecules* **2012**, *45* (12), 5099–5107.
- (9) Guild, J. D.; Knox, S. T.; Burholt, S. B.; Hilton, E. M.; Terrill, N. J.; Schroeder, S. L. M.; Warren, N. J. Continuous-Flow Laboratory SAXS for In Situ Determination of the Impact of Hydrophilic Block Length on Spherical Nano-Object Formation during Polymerization-Induced Self-Assembly. *Macromolecules* **2023**, *56* (16), 6426–6435.
- (10) Li, Z.; Wang, R.; Luo, X.; Zhang, L.; Tan, J. ABC or ACB Triblock Copolymers? Changing the RAFT Group Position in Diblock Copolymer Macro-RAFT Agents Leads to Different PISA Behaviors in RAFT Dispersion Polymerization. *Polym. Chem.* **2024**, *15* (17), 1736–1747.
- (11) Gao, C.; Li, S.; Li, Q.; Shi, P.; Shah, S. A.; Zhang, W. Dispersion RAFT Polymerization: Comparison between the Mono-functional and Bifunctional Macromolecular RAFT Agents. *Polym. Chem.* **2014**, *5* (24), 6957–6966.
- (12) Zhang, X.; Rieger, J.; Charleux, B. Effect of the Solvent Composition on the Morphology of Nano-Objects Synthesized via RAFT Polymerization of Benzyl Methacrylate in Dispersed Systems. *Polym. Chem.* **2012**, *3* (6), 1502–1509.
- (13) Zhou, D.; Dong, S.; Kuchel, P.; Perrier, R.; Zetterlund, P. B. Polymerization Induced Self-Assembly: Tuning of Morphology Using Ionic Strength and pH. *Polym. Chem.* **2017**, *8* (20), 3082–3089.
- (14) Boissé, S.; Rieger, J.; Pembouong, G.; Beaunier, P.; Charleux, B. Influence of the Stirring Speed and CaCl₂ Concentration on the Nano-object Morphologies Obtained via RAFT-mediated Aqueous Emulsion Polymerization in the Presence of a Water-soluble macroRAFT Agent. *J. Polym. Sci., Part A: Polym. Chem.* **2011**, *49* (15), 3346–3354.
- (15) Ding, Z.; Gao, C.; Wang, S.; Liu, H.; Zhang, W. Macro-RAFT Agent Mediated Dispersion Polymerization: The Monomer Concentration Effect on the Morphology of the in Situ Synthesized Block Copolymer Nano-Objects. *Polym. Chem.* **2015**, *6* (46), 8003–8011.
- (16) Parkinson, S. J.; Fielden, S. D. P.; Thomas, M.; Miller, A. J.; Topham, P. D.; Derry, M. J.; O'Reilly, R. K. Harnessing Cytosine for Tunable Nanoparticle Self-Assembly Behavior Using Orthogonal Stimuli. *Biomacromolecules* **2024**, *25* (8), 4905–4912.
- (17) Wan, W.-M.; Pan, C.-Y. Formation of Polymeric Yolk/Shell Nanomaterial by Polymerization-Induced Self-Assembly and Reorganization. *Macromolecules* **2010**, *43* (6), 2672–2675.
- (18) Hochreiner, E. G.; van Ravensteijn, B. G. P. Polymerization-Induced Self-Assembly for Drug Delivery: A Critical Appraisal. *J. Polym. Sci.* **2023**, *61* (24), 3186–3210.
- (19) Lages, M.; Nicolas, J. In Situ Encapsulation of Biologically Active Ingredients into Polymer Particles by Polymerization in Dispersed Media. *Prog. Polym. Sci.* **2023**, *137*, 101637.
- (20) Phan, H.; Cossutta, M.; Houppé, C.; Le Cœur, C.; Prevost, S.; Cascone, I.; Courty, J.; Penelle, J.; Couturaud, B. Polymerization-Induced Self-Assembly (PISA) for in Situ Drug Encapsulation or Drug Conjugation in Cancer Application. *J. Colloid Interface Sci.* **2022**, *618*, 173–184.
- (21) Pearce, A. K.; Wilks, T. R.; Arno, M. C.; O'Reilly, R. K. Synthesis and Applications of Anisotropic Nanoparticles with Precisely Defined Dimensions. *Nat. Rev. Chem.* **2021**, *5* (1), 21–45.
- (22) Truong, N. P.; Quinn, J. F.; Whittaker, M. R.; Davis, T. P. Polymeric Filomicelles and Nanoworms: Two Decades of Synthesis and Application. *Polym. Chem.* **2016**, *7* (26), 4295–4312.
- (23) Geng, Y.; Dalhaimer, P.; Cai, S.; Tsai, R.; Tewari, M.; Minko, T.; Discher, D. E. Shape Effects of Filaments versus Spherical Particles in Flow and Drug Delivery. *Nat. Nanotechnol.* **2007**, *2* (4), 249–255.
- (24) Hadji, H.; Bouchemal, K. Effect of Micro- and Nanoparticle Shape on Biological Processes. *J. Controlled Release* **2022**, *342*, 93–110.
- (25) Zeeshan, A.; Hadji, H.; Khelifa, H.; Bourge, M.; Bouchemal, K. Understanding the Interplay between Surface Properties and the Aspect Ratio of Ellipsoidal Nanomaterials. *Colloids Surf., A* **2024**, *680*, 132680.
- (26) Rieger, J. Guidelines for the Synthesis of Block Copolymer Particles of Various Morphologies by RAFT Dispersion Polymerization. *Macromol. Rapid Commun.* **2015**, *36* (16), 1458–1471.
- (27) Kang, Y.; Pitto-Barry, A.; Willcock, H.; Quan, W.-D.; Kirby, N.; Sanchez, A. M.; O'Reilly, R. K. Exploiting Nucleobase-Containing

Materials – from Monomers to Complex Morphologies Using RAFT Dispersion Polymerization. *Polym. Chem.* **2015**, *6* (1), 106–117.

(28) Yu, Q.; Ding, Y.; Cao, H.; Lu, X.; Cai, Y. Use of Polyion Complexation for Polymerization-Induced Self-Assembly in Water under Visible Light Irradiation at 25 °C. *ACS Macro Lett.* **2015**, *4* (11), 1293–1296.

(29) Yoon, K.-Y.; Lee, I.-H.; Kim, K. O.; Jang, J.; Lee, E.; Choi, T.-L. One-Pot in Situ Fabrication of Stable Nanocaterpillars Directly from Polyacetylene Diblock Copolymers Synthesized by Mild Ring-Opening Metathesis Polymerization. *J. Am. Chem. Soc.* **2012**, *134* (35), 14291–14294.

(30) Boott, C. E.; Gwyther, J.; Harniman, R. L.; Hayward, D. W.; Manners, I. Scalable and Uniform 1D Nanoparticles by Synchronous Polymerization, Crystallization and Self-Assembly. *Nat. Chem.* **2017**, *9* (8), 785–792.

(31) Huo, M.; Song, G.; Zhang, J.; Wei, Y.; Yuan, J. Nonspherical Liquid Crystalline Assemblies with Programmable Shape Transformation. *ACS Macro Lett.* **2018**, *7* (8), 956–961.

(32) Wan, J.; Fan, B.; Thang, S. H. RAFT-Mediated Polymerization-Induced Self-Assembly (RAFT-PISA): Current Status and Future Directions. *Chem. Sci.* **2022**, *13* (15), 4192–4224.

(33) Wang, Y.; Lorandi, F.; Fantin, M.; Matyjaszewski, K. Atom Transfer Radical Polymerization in Dispersed Media with Low-Ppm Catalyst Loading. *Polymer* **2023**, *275*, 125913.

(34) Delaittre, G.; Nicolas, J.; Lefay, C.; Save, M.; Charleux, B. Surfactant-Free Synthesis of Amphiphilic Diblock Copolymer Nanoparticles via Nitroxide-Mediated Emulsion Polymerization. *Chem. Commun.* **2005**, No. 5, 614–616.

(35) Foster, J. C.; Varlas, S.; Coutraud, B.; Jones, J. R.; Keogh, R.; Mathers, R. T.; O'Reilly, R. K. Predicting Monomers for Use in Polymerization-Induced Self-Assembly. *Angew. Chem. Int. Ed.* **2018**, *57* (48), 15733–15737.

(36) Ikkene, D.; Six, J.-L.; Ferji, K. Progress in Aqueous Dispersion RAFT PISA. *Eur. Polym. J.* **2023**, *188*, 111848.

(37) Shen, D.; Shi, B.; Zhou, P.; Li, D.; Wang, G. Temperature-Dependent Ring-Opening Polymerization-Induced Self-Assembly Using Crystallizable Polylactones as Core-Forming Blocks. *Macromolecules* **2023**, *56*, 4814.

(38) Hurst, P. J.; Rakowski, A. M.; Patterson, J. P. Ring-Opening Polymerization-Induced Crystallization-Driven Self-Assembly of Poly-L-Lactide-Block-Polyethylene Glycol Block Copolymers (ROPI-CDSA). *Nat. Commun.* **2020**, *11* (1), 1–12.

(39) Ellis, C. E.; Garcia-Hernandez, J. D.; Manners, I. Scalable and Uniform Length-Tunable Biodegradable Block Copolymer Nanofibers with a Polycarbonate Core via Living Polymerization-Induced Crystallization-Driven Self-Assembly. *J. Am. Chem. Soc.* **2022**, *144* (44), 20525–20538.

(40) Jiang, J.; Zhang, X.; Fan, Z.; Du, J. Ring-Opening Polymerization of N-Carboxyanhydride-Induced Self-Assembly for Fabricating Biodegradable Polymer Vesicles. *ACS Macro Lett.* **2019**, *8* (10), 1216–1221.

(41) Li, H.; Cornel, E. J.; Fan, Z.; Du, J. Chirality-Controlled Polymerization-Induced Self-Assembly. *Chem. Sci.* **2022**, *13* (47), 14179–14190.

(42) Grazon, C.; Salas-Ambrosio, P.; Ibarboue, E.; Buol, A.; Garanger, E.; Grinstaff, M. W.; Lecommandoux, S.; Bonduelle, C. Aqueous Ring-Opening Polymerization-Induced Self-Assembly (ROPISA) of N-Carboxyanhydrides. *Angew. Chem. Int. Ed.* **2020**, *59* (2), 622–626.

(43) Shi, Q.; Chen, Y.; Yang, J.; Yang, J. Ring-Opening Polymerization-Induced Self-Assembly (ROPISA) of Salicylic Acid α -Carboxyanhydride. *Chem. Commun.* **2021**, *57* (86), 11390–11393.

(44) Grazon, C.; Salas-Ambrosio, P.; Antoine, S.; Ibarboue, E.; Sandre, O.; Clulow, A. J.; Boyd, B. J.; Grinstaff, M. W.; Lecommandoux, S.; Bonduelle, C. Aqueous ROPISA of α -Amino Acid N-Carboxyanhydrides: Polypeptide Block Secondary Structure Controls Nanoparticle Shape Anisotropy. *Polym. Chem.* **2021**, *12* (43), 6242–6251.

(45) Bartlett, P. D.; Jones, R. H. A Kinetic Study of the Leuchs Anhydrides in Aqueous Solution. II. *J. Am. Chem. Soc.* **1957**, *79* (9), 2153–2159.

(46) Bartlett, P. D.; Dittmer, D. C. A Kinetic Study of the Leuchs Anhydrides in Aqueous Solution. III. *J. Am. Chem. Soc.* **1957**, *79* (9), 2159–2160.

(47) Beausery, H.; Grazon, C.; Antoine, S.; Badreldin, M.; Salas-Ambrosio, P.; Harrison, S.; Garanger, E.; Lecommandoux, S.; Bonduelle, C. Polypeptide- and Protein-Based Conjugate Nanoparticles via Aqueous Ring-Opening Polymerization-Induced Self-Assembly (ROPISA). *Macromol. Rapid Commun.* **2024**, *45* (14), 2400079.

(48) Morrell, A. H.; Warren, N. J.; Thornton, P. D. The Production of Polysarcosine-Containing Nanoparticles by Ring-Opening Polymerisation-Induced Self-Assembly. *Macromol. Rapid Commun.* **2024**, *45*, 2400103.

(49) Tinajero-Díaz, E.; Judge, N.; Li, B.; Leigh, T.; Murphy, R. D.; Topham, P. D.; Derry, M. J.; Heise, A. Poly(l-Proline)-Stabilized Polypeptide Nanostructures via Ring-Opening Polymerization-Induced Self-Assembly (ROPISA). *ACS Macro Lett.* **2024**, *13*, 1031–1036.

(50) Liu, B.; Fang, R.; Li, W.; Wu, X.; Liu, T.; Lin, M.; Sun, J.; Chen, X. Fast Catalyst-Free Synthesis of Stereoselective Polypeptides via Hierarchical Chiral Assembly. *J. Am. Chem. Soc.* **2024**, *146* (24), 16558–16566.

(51) Xi Huang, S.; Hao Wang, Z.; Lin, M.; Hui Fu, X.; Sun, J. One-Pot Preparation of Polypeptide Nanogels in Aqueous Solution via Ring-Opening Polymerization-Induced Nano-Gelation. *Polym. Chem.* **2023**, *14* (15), 1801–1808.

(52) Tian, L.; Cao, C.; Ho, J.; Stenzel, M. H. Maximizing Aqueous Drug Encapsulation: Small Nanoparticles Formation Enabled by Glycopolymers Combining Glucose and Tyrosine. *J. Am. Chem. Soc.* **2024**, *146* (12), 8120–8130.

(53) Isidro-Llobet, A.; Álvarez, M.; Albericio, F. Amino Acid-Protecting Groups. *Chem. Rev.* **2009**, *109* (6), 2455–2504.

(54) Rodríguez-Hernández, J.; Gatti, M.; Klok, H.-A. Highly Branched Poly(l-Lysine). *Biomacromolecules* **2003**, *4* (2), 249–258.

(55) Feller, D.; Otten, M.; Hildebrandt, M.; Krüsmann, M.; Bryant, G.; Karg, M. Translational and Rotational Diffusion Coefficients of Gold Nanorods Functionalized with a High Molecular Weight, Thermoresponsive Ligand: A Depolarized Dynamic Light Scattering Study. *Soft Matter* **2021**, *17* (15), 4019–4026.

(56) Zandomenighi, G.; Krebs, M. R. H.; McCammon, M. G.; Fändrich, M. FTIR Reveals Structural Differences between Native β -Sheet Proteins and Amyloid Fibrils. *Protein Sci.* **2004**, *13* (12), 3314–3321.

(57) Gavva, V.; Al Musaimi, O.; Bent, C.; Williams, D. R. Determining the Hydrophobicity Index of Protected Amino Acids and Common Protecting Groups. *Separations* **2023**, *10* (8), 456.

(58) Mozhaev, V. V.; Berezin, I. V.; Martinek, K.; Nosoh, Y. Structure-Stability Relationship in Proteins: Fundamental Tasks and Strategy for the Development of Stabilized Enzyme Catalysts for Biotechnolog. *Crit. Rev. Biochem.* **1988**, *23* (3), 235–281.

(59) Calculation of molecular properties and bioactivity score. <https://www.molinspiration.com/cgi/properties> (accessed 11–January–2025).

(60) Karandur, D.; Wong, K.-Y.; Pettitt, B. M. Solubility and Aggregation of Gly5 in Water. *J. Phys. Chem. B* **2014**, *118* (32), 9565–9572.

(61) Bykov, S.; Asher, S. Raman Studies of Solution Polyglycine Conformations. *J. Phys. Chem. B* **2010**, *114* (19), 6636–6641.

(62) Lotz, B. Rippled Sheets: The Early Polyglycine Days and Recent Developments in Nylons. *ChemBiochem* **2022**, *23* (5), No. e202100658.

(63) Taga, K.; Sowa, M. G.; Wang, J.; Etori, H.; Yoshida, T.; Okabayashi, H.; Mantsch, H. H. FT-IR Spectra of Glycine Oligomers. *Vib. Spectrosc.* **1997**, *14* (1), 143–146.

(64) Spyridakou, M.; Tzourtouklis, I.; Graf, R.; Beausery, H.; Bonduelle, C.; Lecommandoux, S.; Floudas, G. Multiple Levels of

Organization in Amphiphilic Diblock Copolymers Based on Poly(γ -Benzyl-L-Glutamate) Produced by Aqueous ROPISA. *Biomacromolecules* **2025**, *26*, 1892.

(65) Hurst, P. J.; Graham, A. A.; Patterson, J. P. Gaining Structural Control by Modification of Polymerization Rate in Ring-Opening Polymerization-Induced Crystallization-Driven Self-Assembly. *ACS Polym. Au* **2022**, *2* (6), 501–509.

(66) Lecommandoux, S.; Achard, M.-F.; Langenwalter, J. F.; Klok, H.-A. Self-Assembly of Rod–Coil Diblock Oligomers Based on α -Helical Peptides. *Macromolecules* **2001**, *34* (26), 9100–9111.

(67) Palermo, N. Y.; Csontos, J.; Murphy, R. F.; Lovas, S. The Role of Aromatic Residues in Stabilizing the Secondary and Tertiary Structure of Avian Pancreatic Polypeptide. *Int. J. Quantum Chem.* **2008**, *108* (4), 814–819.

(68) Lanzarotti, E.; Biekofsky, R. R.; Estrin, D. A.; Marti, M. A.; Turjanski, A. G. Aromatic-Aromatic Interactions in Proteins: Beyond the Dimer. *J. Chem. Inf. Model.* **2011**, *51* (7), 1623–1633.

(69) Liu, X.; Fan, R.; Lu, B.; Le, Y. Polypeptides Micelles Composed of Methoxy-Poly(Ethylene Glycol)-Poly(L-Glutamic Acid)-Poly(L-Phenylalanine) Triblock Polymer for Sustained Drug Delivery. *Pharmaceutics* **2018**, *10* (4), 230.

(70) Bossion, A.; Nicolas, J. Synthesis of Poly(Asparagine-Co-Phenylalanine) Copolymers, Analogy with Thermosensitive Poly(Acrylamide-Co-Styrene) Copolymers and Formation of PEGylated Nanoparticles. *Eur. Polym. J.* **2020**, *140*, 110033.

(71) Aydinlioglu, E.; Abdelghani, M.; Le Fer, G.; van Hest, J. C. M.; Sandre, O.; Lecommandoux, S. Robust Polyion Complex Vesicles (PICsomes) Based on PEO-b-Poly(Amino Acid) Copolymers Combining Electrostatic and Hydrophobic Interactions: Formation, siRNA Loading and Intracellular Delivery. *Macromol. Chem. Phys.* **2023**, *224* (1), 2200306.

(72) Gu, X.; Qiu, M.; Sun, H.; Zhang, J.; Cheng, L.; Deng, C.; Zhong, Z. Polytyrosine Nanoparticles Enable Ultra-High Loading of Doxorubicin and Rapid Enzyme-Responsive Drug Release. *Biomater. Sci.* **2018**, *6* (6), 1526–1534.

(73) Gu, X.; Wei, Y.; Fan, Q.; Sun, H.; Cheng, R.; Zhong, Z.; Deng, C. cRGD-Decorated Biodegradable Polytyrosine Nanoparticles for Robust Encapsulation and Targeted Delivery of Doxorubicin to Colorectal Cancer *in Vivo*. *J. Controlled Release* **2019**, *301*, 110–118.

(74) Bastiat, G.; Plourde, F.; Motulsky, A.; Furtos, A.; Dumont, Y.; Quirion, R.; Fuhrmann, G.; Leroux, J.-C. Tyrosine-Based Rivastigmine-Loaded Organogels in the Treatment of Alzheimer's Disease. *Biomaterials* **2010**, *31* (23), 6031–6038.

(75) Costache, M. C.; Vaughan, A. D.; Qu, H.; Ducheyne, P.; Devore, D. I. Tyrosine-Derived Polycarbonate-Silica Xerogel Nanocomposites for Controlled Drug Delivery. *Acta Biomater.* **2013**, *9* (5), 6544–6552.

(76) Tiwari, P.; Basu, A.; Sahu, S.; Gound, S.; Christman, R. M.; Tiwari, A. K.; Trivedi, P.; DuttKonar, A. An Auxin–Tyrosine Derivative Based Biocompatible Supergelator: A Template for Fabrication of Nanoparticles for Sustained Release of Model Drugs. *New J. Chem.* **2018**, *42* (7), 4915–4922.

(77) Huang, J.; Hastings, C. L.; Duffy, G. P.; Kelly, H. M.; Raeburn, J.; Adams, D. J.; Heise, A. Supramolecular Hydrogels with Reverse Thermal Gelation Properties from (Oligo)Tyrosine Containing Block Copolymers. *Biomacromolecules* **2013**, *14* (1), 200–206.

(78) Kambale, P.; Nisal, R.; Jayakannan, M. Synthetic Strategy to Build High-Molecular-Weight Poly(L-Tyrosine) and Its Unexplored β -Sheet Block Copolymer Nanoarchitectures. *Biomacromolecules* **2025**, *26* (4), 2580–2600.

(79) Jiang, C.; Zhao, C.; Xu, P.; Song, Q.; Tao, X.; Lin, S. Effects of Secondary Structures and pH on the Self-Assembly of Poly(Ethylene Glycol)-b-Polytyrosine. *Biomacromolecules* **2024**, *25*, 5028.



CAS INSIGHTS™

EXPLORE THE INNOVATIONS
SHAPING TOMORROW

Discover the latest scientific research and trends with CAS Insights. Subscribe for email updates on new articles, reports, and webinars at the intersection of science and innovation.

Subscribe today

CAS
A division of the
American Chemical Society